UNIVERSIDAD DISTRITAL
FRANCISCO JOSÉ DE CALDAS

UD y la GEOMÁTICA

Multispectral image classification from axiomatic locally finite spaces-based segmentation

Clasificación de imágenes multiespectrales a partir de segmentación basada en espacios axiomáticos localmente finitos

José Valero[1] & Iván Lizarazo[2]

ABSTRACT

Geographical object-based image analysis (GEOBIA) usually starts defining coarse geometric space elements, i.e. image-objects, by grouping near pixels based on (a, b)-connected graphs as neighbourhood definitions. In such an approach, however, topological axioms needed to ensure a correct representation of connectedness relationships can not be satisfied. Thus, conventional image-object boundaries definition presents ambiguities because one-dimensional contours are represented by two-dimensional pixels. In this paper, segmentation is conducted using a novel approach based on axiomatic locally finite spaces (provided by Cartesian complexes) and their linked oriented matroids. For the test, the ALFS-based image segments were classified using the support vector machine (SVM) algorithm using directional filter response as an additional channel. The proposed approach uses a multi-scale approach for the segmentation, which includes multi-scale texture and spectral affinity analysis in boundary definition. The proposed approach was evaluated comparatively with conventional pixel representation on a small subset of GEOBIA2016 benchmark dataset. Results show that classification accuracy is increased in comparison to a conventional pixel segmentation.

Keywords: GEOBIA, inter-pixel element, finite spaces, oriented matroid, SVM classification

RESUMEN

El análisis de imagenes basado en objetos geográficos (GEOBIA por su sigla en inglés) comienza generalmente definiendo elementos más gruesos del espacio geométrico u objetos de imagen, agrupando píxeles cercanos con base en grafos (a, b)-conectados como definiciones de vecindario. En este enfoque, sin embargo, pueden no cumplirse algunos axiomas topológicos requeridos para garantizar una correcta representación de las relaciones de conexión. Por lo tanto, la definición convencional de límites de objetos de imagen, presenta ambigüedades debido a que los contornos unidimensionales están representados por píxeles bidimensionales. En este trabajo, la segmentación se lleva a cabo mediante un nuevo enfoque basado en espacios axiomáticos localmente finitos (proporcionados por complejos cartesianos) y sus matroides orientados asociados. Para probar el enfoque propuesto, los segmentos de la imagen basada en ALFS fueron clasificados usando el algoritmo de máquina de soporte vectorial (SVM por su sigla en inglés) usando la respuesta a filtros direccionales como un canal adicional. El enfoque propuesto utiliza un enfoque multiescala para la segmentación, que incluye análisis de textura y de afinidad espectral en la definición de límite. La propuesta se evaluó comparativamente con la representación de píxeles convencionales en un pequeño subconjunto del conjunto de datos de referencia GEOBIA2016. Los resultados muestran que la exactitud de la clasificación se incrementa en comparación con la segmentación convencional de pixeles.

Palabras clave: GEOBIA, elemento inter-pixel, espacios finitos, matroide orientado, clasificación SVM.

1   Universidad Distrital Francisco José de Caldas–Carrera 7 No. 40B – 5, Bogotá, Colombia – Correo electrónico: jvalero@udistrital.edu.co

2   Universidad Nacional de Colombia–Carrera 45 # 26-85, Bogotá, Colombia – Correo electrónico: ializarazos@unal.edu.co

Introduction

GEOBIA based image classification usually uses a given nearby pixel grouping scheme (Grady, 2012; Brun *et al.,*2003) to form elements of coarser grain (image-objects) which are then used as spatial units to apply a classification model. In this first segmentation stage, a common strategy is to group near pixels based on (a, b)-connected graphs to represent neighbourhood relationships. However, some ambiguities appear using such representation as topological requirements are not respected (Kovalevsky, 2008). Specifically, digital image segmentation is heavily dependent on appropriate boundary definitions, also known as T_0, which are very hard to obtain in a 2D space from 2D-elements as (a, b)-connected graphs (Kovalevsky, 1989). For such a purpose, Kovalevsky (1984); (2001); (2005); (2006), proposes the use of Axiomatic Locally Finite Space (ALFS) provided by Cartesian complexes which rely on Abstract Cell Complexes (ACC). The ALFS digital space meets the T_0 separation property by defining properly the boundary of higher dimension space elements by connecting lower dimension elements.

Valero *et al.,* (2017) proposed a computational framework based on Cartesian complexes as well as a codification of topological and geometrical features using oriented matroids (Whitney, 1935; Oxley, 2006) linked with the hyperplane central arrangement (Fukuda, 2004) defined by Standard Separating Forms (SSFs) (Kovalevsky, 2008) available in the Cartesian complex (CC) geometric space. However, such framework does not include neither the spectral affinity analysis (Arbeláez *et al.,* 2011) nor the multi-scale criteria when using oriented gradient for producing image-objects.

This paper assesses a novel segmentation approach based on the image segmentation procedure stablished by Arbeláez *et al.,* (2011), but using a multispectral image represented as a CC. Proposed segmentation approach starts with a grey scale image conversion based on the covariance matrix. Then, filter and gradient kernels are built from SSFs defined on each outermost 1-cell. It is followed by the affinity analysis using the decimating procedure introduced in Pont-Pont-Tuset *et al.,* (2015), but using inter-pixel 1-cells. For the affinity analysis, multi-scale gradients on each multispectral band and texture layer are used. Later, support vector machines algorithm (SVM) (Tso and Mather, 2009) classify the produced image-objects.

This paper is organized as follows. Section 2 describes the dataset used. Section 3 explains the proposed method. Results and discussion are presented in Section 4 and conclusions are drawn in Section 5.

Data

A subset of the airborne image dataset provided by International Society for Photogrammetry and Remote Sensing (ISPRS) for the 2D Semantic Labelling contest was used in this study. The dataset consists of high resolution true orthophoto (TOP) tiles over Potsdam, a historic city in Germany. The TOP tiles are 8-bit TIFF files with four bands: RGBIR (R-G-B-IR). Images cover urban scenes that have been classified manually into six land cover classes: Building, Low vegetation, Tree, Car, Impervious surfaces, and Clutter/background. In this study, tile 40_10 was selected for classification. Two non-overlapping 1000×1000 pixel windows were subset, one from (5001, 1) to (6000, 1000) for training (Figure 1(a)) and the other one from (2501, 5001) to (3500, 6000) for validation (Figure 1(b)).

Methods

The main purpose of the present work is to evaluate if the representation of an image in terms of Cartesian complexes (Kovalevsky, 2008) allows a good segmentation and if the 1-dimensional interpixel element based directional filter response inclusion allows to improve SVM classification having an additional variable.

(a)   (b)

FIGURE 1: Orthophoto´s true colour composition: (a) training, (b) test windows

Therefore, the proposed approach comprised two stages: (i) image-object production (i.e. image segmentation) and (ii) segment-based SVM classification. The workflow for multispectral image segmentation and subsequent classification is shown in figure 2. To compare the additional variable inclusion (directional filter response) two classification scenarios were tested: (i) using only the four bands as input; and (ii) using directional filtering response as additional input band.

The assessment comprises carrying out the entire process of segmentation and classification of the image in both representations, i.e. the Cartesian complex-based image segmentation and its subsequent SVM-based classification and a conventional image segmentation (Arbeláez *et al.,* 2011) and its subsequent SVM-based classification.

Although the digital elevation model was available, it was not used because this study only compares conventional pixel and Cartesian complex image representations.

Image-object production stage

The image-object production stage comprised 10 tasks, which are described below, proposed by Arbeláez *et al.,* (2011). However, these tasks were conducted on 1-cell inter-pixel space elements, based on Cartesian complexes (CC), rather than on the conventional space of pixels. The segment Cartesian complex so obtained was used as super pixels (image-objects) input for subsequent classification stage.

CC (1) and grey scale (2) conversions

First, it is necessary the image conversion from the conventional pixel space to the CC-based space (step 1) for having available inter pixel space elements. It followed the procedure described in Kovalevsky (2008) applying the EquNaLi set membership rule (Kovalevsky, 1989) on-the-fly when an inter-pixel element (1-cells) was needed. Figure 3(a) shows a 5×5 color 2D toy image which, as a 2D Cartesian complex, is graphically represented including inter–pixel space elements.

A 2–cell in a Cartesian complex corresponds to a pixel of the 2D image, while the lower dimensional cells correspond to the inter–pixel elements that do not exist in the 2D image. In figure 3(b), a 2–cell is represented as a square area, each 1–cell is represented as a vertical or horizontal dark segment line corresponding to the inter–pixel element between the two respective pixels, and each 0–cell is represented as a black dot corresponding to the inter–pixel element in the centre of the four respective pixels.

The finite space is completed with lower dimensional cells on the boundary of it. While the representation of figure 3(b) is intuitive, this suggests a non-existent "density" in a locally finite space; for this reason, it is preferred the one given in figure 3(c). There each cell of any dimension is represented as a dot and differentiated by its combinatorial coordinates but in the figure has been used colours, the same as in Figure 3(b), because the combinatorial coordinates are not shown.
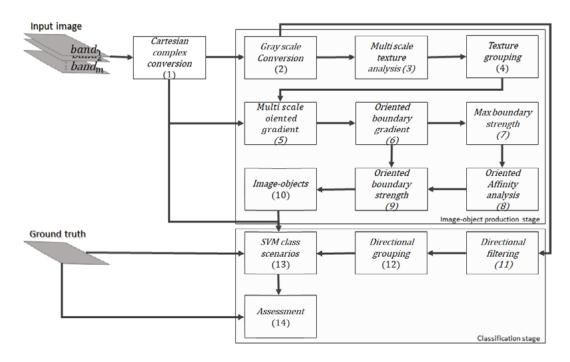

FIGURE 2. Cartesian complex-based multispectral image segmentation and SVM-based classification workflow
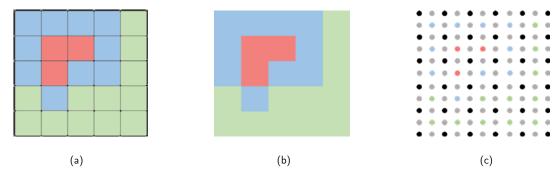
FIGURE 3. A 2D image represented in a 2D Cartesian complex. (a) A colour image. (b) Image with inter-pixel elements included. (c) Digital representation as an abstract cell finite set

In computer vision, the luminance provides more information in distinguishing visual features, so it is preferred as filtering input. To obtain a single grey scale image from the multispectral CC image, a linear combination of all bands was proposed and computed based on the level of information provided by each band using the covariance matrix (Tso and Mather, 2009). The contribution of each band was calculated by means of equation 1.

$$w_l = \frac{1}{\sum_{i=1}^{n} \sum_{j=1}^{n} cov_{i,j}} \sum_{i=1}^{n} cov_{i,l} \,, \qquad (1)$$
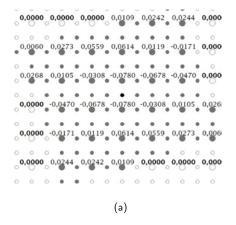
where $cov_{i,j}$ and $cov_{i,l}$ are the covariance between bands i and j or l, n is the number of bands and $l = 1,2,...,n$. The computed weights for the training image were $w_1 = 0.48$, $w_2 = 0.25$ and $w_3 = 0.26$, while for the test image were $w_1 = 0.51$, $w_2 = 0.23$ and $w_3 = 0.26$.

Multiscale texture analysis (3) and Texture grouping (4)

A texture analysis was performed to reduce the risk that differences in contrast due to the texture of the area to be delimited are considered borders. Filter banks for texture recognition (Leung and Jitendra, 1996) were used in the filtering task, but using a central 1-cell. Each filter bank was composed by Gaussian derivative filter kernels each with an orientation, a radius around the central 1-cell and a granularity scale. Orientations were defined from SSFs available in a SSF central arrangement (Fukuda, 2004) (see Section 3.1.3). Filter kernels with $(2n+1) \times 2n$ 2-cells (pixels) were used, where n is the number of 1-cells from the central one. Figure 4(a) shows a rotated Gaussian filter kernel (biggest dots are 2-cells, smallest dots are inter-pixel elements and the black one is the central 1-cell) and its application on a small portion of the training image (figure 4(b)). The figure shows that, when the initial kernel (horizontal along central 1-cell) is rotated, the new kernel is extended and completed with zeroes in such a way that it contains the rotated evaluation kernel (filled dots). In this study, as in Arbeláez *et al.,* (2011), a filter bank with 2 scales (n=3, 3 √2) and 8 orientations was used for the texture analysis, but on each inter-pixel 1-cell.

After multiscale texture analysis, each 1-cell received a response vector with 8 values (the number of filter kernels in the filter bank). Those response vectors were grouped using the k-means clustering technique to produce an image texture with 32 texture classes. The texture class centres were first calculated for the training window texture analysis and after applied to the test window texture analysis.
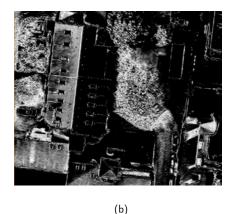

(a)

(b)

FIGURE 4. π\10 rotated second derivative Gaussian filter kernel (a) and its outcome when applied to a little portion of training window (b)

Multiscale oriented gradient (5)

Boundaries correspond to image discontinuities, so it would be expected that a large distance between the local histogram on each side, along a given orientation, should be an indicator of being in one of them (Arbeláez *et al.,* 2011). For each scale, the oriented gradient calculation began defining a Manhattan distance based ball (Worboys and Duckham, 2004), which was centred at a 1-cell. Each ball was overlaid with a SSF central arrangement to produce a sector set (figure 5(a)). Then, for each sector, its histogram was calculated and then, it was combined with the others sector histograms on the same side in agreement with a given orientation (figure 5(b)). The oriented gradient image was computed for each 1-cell placing at it a ball split in two half balls along each SSF orientation.

In Valero *et al.,* (2017), the SSF set is produced passing each SSF over each 0-cell and the central 1-cell but this causes that the inner defined SSFs are contained by one or several outermost. In this study, the SSFs were obtained in such a way that each one crossed both an external 1-cell and a central one. Therefore, the maximum number of SSFs was obtained combinatorically from SSF, where n is a radius in number of cracks from the central one. Oriented matroids (Whitney, 1935; Oxley, 2006) were used to produce indices for sectors considering that each SSF subdivides the space in three subsets (the inter-pixel elements located on that SSF and the space elements located on each side). Equation 2 was used to transfer the SSF geometry to its associated sign.

$$\delta(c)_i = \begin{cases} -, & H_i(c) < -|m| \\ +, & H_i(c) > |m| \\ 0, & \text{otherwise} \end{cases} \qquad (2)$$

where c is a 1-cell, $H_i(c)$ is *i*th SSF value at *x,y* combinatorial coordinate of c, $H(x,y) = ax + by + l$ (Kovalevsky, 2008) and $m = a$ if c is a vertical 1-cell or b if c is a horizontal one.

The position vector (De Loera *et al.,* 2010) δ(c) of each 1-cell and its sector index were calculated as in Valero *et al.,* (2017), but applying equation 2 for each SSF in the central arrangement (see figure 5(a). For a given orientation, only the 1-cell elements on each SSF side were considered (shown as black dots in figure 5(b).

Oriented boundary gradient (6) and Maximum boundary strength (7)

In order to obtain a geometrical measurement of oriented boundary strength, the oriented gradient images calculated for each scale based on balls of several radii from the finest to the coarser were linearly combined for producing the oriented boundary gradient using equation 3.

$$G(c,\theta) = \frac{1}{n_s} \sum_{i=1}^{n_s} G_i(c,\theta) \qquad (3)$$

Where c is a CC 1-cell element, s is the number of scales, θ is an orientation and i is the oriented gradient at i scale. Then, the oriented boundary gradient image was used for finding the maximum gradient value G(C) = maxθ (G(c, θ)) $G(c) = \max_\theta (G(c,\theta))$

Oriented affinity analysis (8)

An affinity analysis based spectral boundary strength was done as by Arbeláez *et al.* (2011), but between pairs of 1-cell elements inside an affinity area. The affinity area was defined using a Manhattan distance based ball. The search started with the smallest ball (only a 1-cell from the central one) computing each time the affinity between each external 1-cell and the central one. Next, the search proceeded in an iterative process expanding the ball by a 1-cell in all directions each time. Then, it was computed the affinity between each updated external 1-cell and its previous 1-cell that was in the same SSF from the central 1-cell (this is shown in figure 6(a)). While the ball expanded, *W* and *D* sparse matrices were progressively calculated.

Next, *W* and *D* matrices were used to calculate eigenvector images using the decimated procedure and software developed by Pont-Tuset *et al.,* (2015). Then, a filter bank of oriented first derivative Gaussian kernels was applied. Finally, filtered eigenvector channels were linearly combined by orientation to produce the oriented affinity image. Figure 6(b) shows the oriented affinity outcome for a small portion of the training window by the most horizontal orientation.
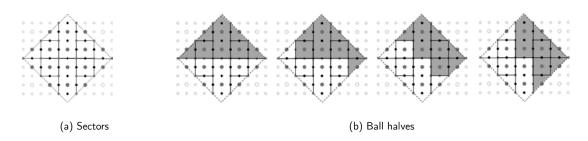

(a) Sectors

(b) Ball halves

FIGURE 5: Common sectors in a 7-SSF central arrangement (a), and their combination for four SSF orientations (b)

Oriented boundary strength (9) and Image-object (10) production

The oriented gradient images calculated for each scale along with the oriented affinity image were linearly combined by orientation for producing the oriented global boundary strength using Equation 4.
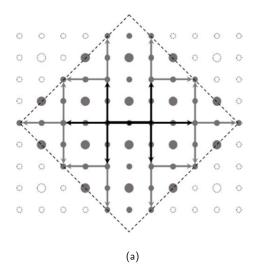
$$G_s(c,\theta) = \frac{1}{n_s + 1}\left(G_a(c,\theta) + \sum_{i=1}^{n_s} G_i(c,\theta)\right) \qquad (4)$$

Where c is a CC 1-cell element, ns is the number of scales, is an orientation, G_i is the oriented gradient at *i* scale and *Ga* is the oriented affinity. The maximum boundary strength image $\max_\theta\left(G_s(c,\theta)\right)$ was used as input for a segmentation based on a 2-levels watershed transform (Valero *et al.*, 2017) and its outcome was taken as image-object input for the classification stage.

Classification stage

Directional filtering (11) and grouping (12)

Besides spectral channels, a directional filter response analysis was applied to produce an additional channel. First, a bank of filter for 8 orientations was produced from an SSF central arrangement. As in Section 3.1.3, at each 1-cell a ball split in two halves was placed along each SSF orientation to produce a directional filter kernel (figure 7) assigning to each 2-cell in the half ball the respective sign based on equation 2. Then, this bank filter was applied to the grey scale image (obtained in Section 3.1.1) to produce at each 1-cell a response vector with as many values as the number of filter kernels in the filter bank. Next, as in section 3.1.2 these response vectors were grouped using the k-means clustering technique to produce a response class image that was used as an additional SVM classification variable.
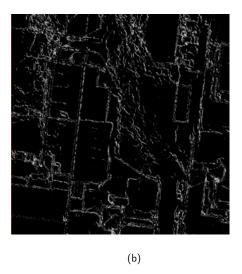

(a)

(b)

FIGURE 6: Affinity search area defined using a Manhattan distance based ball (a) and the most horizontal affinity CC calculated from all filtered eigenvectors (b)
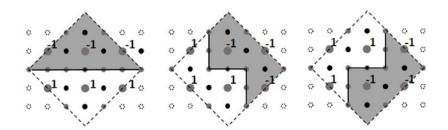

FIGURE 7: Kernels used in directional filtering

SVM-based classification scenarios (13) and accuracy assessment (14)

The procedure described in Section 3.1 was applied to both training and test windows to produce the respective image-object Cartesian complexes. Mean values of input bands and directional filter response additional channel were used as image-object features. Two classification scenarios were tested: (i) using only the four bands as input; and (ii) using directionally filtered images as additional input bands. Both conventional and CC space representation were tested at each scenario. Training and test reference classification images are shown in figure8, blue areas correspond to Building category, cyan to Low vegetation, green to Tree, yellow to Car and white to Impervious surfaces. Image classification and accuracy assessment processes comprised four steps: (i) Stratified sampling based training (table 1), (ii) Radiometric statistics calculation and SVM (one versus others)-based classification model training, (iii) SVM-based classifications, and (iv) thematic accuracy evaluation.

TABLE 1. Number of training and testing points at each thematic category

Class	Training	Testing
Building	11651	479851
Impervious surfaces	6788	133712
Tree	5247	202528
Low vegetation	3320	133938
Clutter/background	2311	36497
Car	683	13474
Total	30000	1000000

Results and discussion

Figure 9 shows classified images obtained based on four spectral bands plus directional filtering responses (scenario 2), for both conventional (left) and CC representations (right).
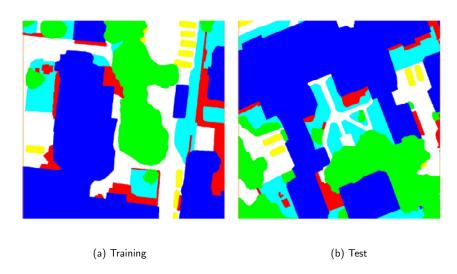

(a) Training

(b) Test

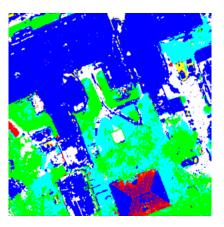**FIGURE 8:** ISPRS Reference classification images

FIGURE 9. SVM-based classification obtained from spectral channels plus directional filters for conventional (left) and CC (right) representations.

In tables 2 and 3, rows correspond to reference classification and columns to obtained classification. These tables show SVM-based classification error matrices (reference weighted in percentage) for conventional and CC representations based only on the multispectral feature space (table 3 and conventional and CC representations based on the feature space extended with directional filter (Table 1). The overall accuracy for each classification and their respective 95% confidence intervals (Tang *et al.,* 2004) were calculated from the error matrices (see table 4).

As can be seen in table 4 for scenario 2 the overall accuracy of the classification is slightly improved when the representation space based on the Cartesian complexes is used. Although the general improvement is not significant, the inclusion of the multi-scale factor both in the texture analysis and in the calculation of the oriented gradients was definitive to produced CC-based image-objects comparable with those obtained from the conventional representation. The use of Cartesian complex-based watershed transform using multiscale texture and multispectral gradients and affinity analysis favoured the proper definition of super pixels resulting in just a small decrease in the classification overall accuracy (scenario 1).

On the other hand, when the directional filtering grouping feature was used, the general accuracy value of the classification was slightly higher. This increase is small

TABLE 2. Error matrix for classification based on four spectral channels
for conventional (1) and CC (2) representations

Category	Building		Impervious surface		Tree		Low vegetation		Clutter/ background		Car	
	(1)	(2)	(1)	(2)	(1)	(2)	(1)	(2)	(1)	(2)	(1)	(2)
Building	**82.0**	**82.3**	5.8	6.3	1.4	1.4	4.0	4.5	6.3	3.3	0.6	2.2
Impervious surfaces	30.7	36.8	**43.1**	**35.3**	11.0	13.0	13.6	12.4	1.3	1.8	0.3	0.6
Tree	2.5	3.2	1.9	2.1	**55.6**	**56.3**	39.6	38.1	0.2	0.1	0.2	0.2
Low vegetation	1.6	3.3	1.8	1.8	43.6	43.2	**52.9**	**51.5**	0.2	0.1	0.0	0.0
Clutter/background	22.9	27.0	12.2	14.7	12.4	12.4	44.9	38.1	**1.1**	**1.3**	6.5	6.6
Car	50.0	54.2	14.9	11.1	0.0	0.0	4.1	3.6	3.1	2.4	**27.9**	**28.7**

TABLE 3. Error matrix for classification based on four spectral channels plus directional filters
for conventional (1) and CC (2) representations.

Category	Building		Impervious surface		Tree		Low vegetation		Clutter/ background		Car	
	(1)	(2)	(1)	(2)	(1)	(2)	(1)	(2)	(1)	(2)	(1)	(2)
Building	**84.0**	**81.7**	5.0	8.4	1.4	2.5	3.9	2.6	4.4	4.2	1.3	0.6
Impervious surfaces	33.2	17.7	**41.7**	**58.5**	12.0	10.5	12.3	10.7	0.5	2.0	0.3	0.7
Tree	2.8	2.7	2.3	2.9	**57.9**	**61.5**	36.9	32.6	0.1	0.2	0.1	0.1
Low vegetation	1.7	3.2	2.0	2.2	47.6	42.2	**48.6**	**52.2**	0.0	0.2	0.0	0.0
Clutter/background	24.5	30.8	10.8	12.4	12.8	17.7	44.7	35.9	**0.6**	**1.8**	6.6	1.5
Car	50.6	59.4	13.5	9.3	0.2	0.0	4.4	3.1	3.1	1.3	**28.2**	**26.7**

TABLE 4. Overall thematic accuracy and confidence intervals for the SVM-based classification.

Features	Space representation	Overall accuracy	95% confidence interval	
			Minimum	Maximum
Spectral only	Conventional	63.86	22.81	73.77
	CC	62.95	21.15	71.93
Spectral +	Conventional	64.51	23.29	74.28
directional filtering	CC	66.87	27.38	78.24

with respect to the result obtained from the classification based only on the spectral features since the response is scale dependent (Leung and Jitendra, 1996) and therefore, resulting classes are mixed depending on the combination of objects with different scales and texture patterns. It is not the case of Building class, which was the class that always became confused less than 20% in conventional or CC representations.

In spite that the assessment stage was conducted against the whole reference classification (i.e. an image composed by 1000000 pixels), the overall accuracy always was higher than 60%. As shown in table 4, the use of a CC space representation and a feature space extended with directional filtering response grouping produced a slight but progressive increase in overall accuracy, which is improved from 62.95%, in the CC representation with only spectral features, up to 66.87%, in the representation based on CC including all features. This means an improvement in the overall accuracy of 3.92% (scenario 2).

Conclusions

Results from this study show that the Cartesian complex-based image classification, based on the Cartesian complex space, allows to improve the accuracy by class for the classification based on feature space extended with directional filters responses. Results also suggest that the inclusion of additional, directionally filtered bands, not always improve thematic accuracy due to the scale dependence of directional filtering.

The availability of an underlying Cartesian complex space provides a topologically correct oriented gradient calculation. In a conventional space when a disk is defined it is recommended not using the pixel linear arrangement which meets the diameter along the orientation as it does not lay in any of two sides but in the orientation. However, in a complex Cartesian space, there are interpixel elements that allow representing this situation properly by modelling that dividing line based on 1-cells and not on pixels, so it is possible use all 2-cell. The availability of an underlying CC space provides a topologically correct affinity analysis. In contrast to the conventional representation based only on pixels, the existence of inter-pixel elements allows an adequate affinity assessment along a connecting line whose representation is made from a SSF (1-cell elements).

While results of the experiments show that, the benefits of the inclusion of an underlying space based on CC are not significant, the possibility to fulfil topological requirements suggest that the Cartesian complex-based image analysis framework is worth of further development. Authors will explore options to reformulate several processing tasks based on Cartesian complexes to produce better outcomes. This includes fitting cylindrical parabolas to elliptical patches at each 1-cell after computing oriented gradient to counteract the phantom border effect (i.e. to avoid producing borders which do not exist) (Malik *et al.,* 2001).

Bibliography

Arbeláez P., Maire M., Fowlkes C., Malik J.(2011). Contour Detection and Hierarchical Image Segmentation. *IEEE Trans. Pattern Anal. Mach. Intell,* vol. 33, n° 5, p. 898–916.

Brun L., Domenger J-P, Mokhtari M. (2003). Incremental modifications of segmented image defined by discrete maps. *Journal of Visual Communication and Image Representation,* vol. 14, no 3, p. 251 – 290, http://www.sciencedirect.com/science/article/pii/S1047320303000233.

Cramer M. (2010). *The DGPF-Test on Digital Airborne Camera Evaluation Overview and Test Design,* http://www.ifp.uni-stuttgart.de/dgpf/DKEP-Allg.html.

De Loera J. A., Rambau J., Santos F. (2010). *Triangulations: Structures for Algorithms and Applications*. First ed. Springer Publishing Company, Incorporated.

Fukuda K. (2004). *Lecture notes on oriented matroids and geometric computation*. Technical Report. RO-2004.0621, course of Doctoral school in Discrete System Optimization, EPFL 2004.

Grady L. (2012). *Targeted image segmentation using graph methods*. Department of Image Analytics and Informatics Siemens Corporate Research Princeton, NJ. http://citeseerx.ist.psu.edu/viewdoc/download?doi=10.1.1.303.7046&rep=rep1&type=pdf

Kovalevsky V.A. (2005). Algorithms in Digital Geometry Based on Cellular Topology. *Proceedings. Springer Berlin Heidelberg,* p. 366–393.

Kovalevsky, V.A. (1989). Finite Topology as Applied to Image Analysis. In *Computer Vision, Graphics, and Image Processing*, vol. 42 n° 2, p. 141–161.

Kovalevsky V. A. (2001). Algorithms and Data Structures for Computer Topology, In: Bertrand G., Imiya A., Klette R. (eds) Digital and Image Geometry. *Lecture Notes in Computer Science*, vol. 2243. Springer, Berlin, Heidelberg, p. 38-58.

Kovalevsky V. A. (2006). Axiomatic Digital Topology. *Journal of Mathematical Imaging and Vision*, vol. 26, n° 1-2, p. 41–58.

Kovalevsky V. A. (1984). Discrete Topology and Contour Definition. *Pattern Recognition Letters,* vol. 2, n° 5, p. 281-288.

Kovalevsky V. A. (2008). Geometry of Locally Finite Spaces. *International Journal of Shape Modelling,* vol. 14 n° 02, p. 231–232.

Leung T. K., Jitendra M. (1996). Detecting, Localizing and Grouping Repeated Scene Elements from an Image. *Proceedings of the 4th European Conference on Computer Vision. ECCV '96, London, UK*, vol 1, p. 546–555. Springer-Verlag.

Malik J., Belongie S., Leung T., Shi J. (2001). Contour and Texture Analysis for Image Segmentation. *International Journal of Computer Vision*, vol. 43, n°, p. 7–27.

Oxley J. G. (2006). *Matroid Theory (Oxford Graduate Texts in Mathematics)*. New York, NY, USA. Oxford University Press, Inc

Pont-Tuset J., Arbeláez P., Barron J. T., Marqués F., Malik J. (2015). *Multiscale Combinatorial Grouping for Image Segmentation and Object Proposal Generation*. CoRR abs/1503.00848. http://arxiv.org/abs/1503.00848.

Tang Pang-Ning, Steinbach M., Kumar V. (2004). *Introduction to Data Mining*, (First Edition). Boston, MA, USA: Addison-Wesley Longman Publishing Co., Inc.

Tso B., Mather P. (2009). *Classification Methods for Remotely Sensed Data*. CRC Press, Taylor & Francis Group.

Valero J., Arbeláez P., Lizarazo I. (2017). A Combinatorial Approach for Hyperspectral Image Segmentation. *Cham: Springer International Publishing.AG 2017*, p. 334–348

Whitney H. (1935). On the abstract properties of linear dependence *American Journal of Mathematics*, vol. 57, p. 509–533.

Worboys M., Duckham M. (2004). GIS: A Computing Perspective, 2nd Edition. Boca Raton, FL, USA: CRC Press, Inc.